Nano Energy 61 (2019) 236–244

Contents lists available at ScienceDirect

Nano Energy

journal homepage: www.elsevier.com/locate/nanoen

Full paper

Flash-induced ultrafast recrystallization of perovskite for flexible light-emitting diodes

Dong Hun Jung[a,1], Jung Hwan Park[c,1], Han Eol Lee[b], Jinwoo Byun[a], Tae Hong Im[b], Gil Yong Lee[a], Jae Young Seok[d], Taeyeong Yun[a], Keon Jae Lee[b,**], Sang Ouk Kim[a,*]

[a] National Creative Research Initiative Center for Multi-Dimensional Directed Nanoscale Assembly, Department of Materials Science and Engineering, KAIST, 291 Daehak-ro, Yuseong-gu, Daejeon, 34141, Republic of Korea
[b] Department of Materials Science and Engineering, KAIST, 291 Daehak-ro, Yuseong-gu, Daejeon, 34141, Republic of Korea
[c] Department of Mechanical Engineering, University of California, Berkeley, CA, 94720, United States
[d] Department of Mechanical Engineering, KAIST, 291 Daehak-ro, Yuseong-gu, Daejeon, 34141, Republic of Korea

ARTICLE INFO

Keywords:
Perovskite
Recrystallization
Flash
Light-emitting diode
Flexible electronics

ABSTRACT

We report ultrafast recrystallization of perovskite (methylammonium lead tribromide, $MAPbBr_3$) by flash light annealing (FLA) for light-emitting diode (LED) application. Intense near-infrared (NIR) peak spectrum (830 and 900 nm) of flash light could rapidly heat $MAPbBr_3$ based LED structures over ~320 °C without radiative damage. Cuboidal morphology of the perovskite active layer was evolved into the dense recrystallized structure with a noticeably small grain size (~38 nm) by FLA, which significantly promoted the radiative recombination. Surface roughness (root mean square (RMS)) of the perovskite layer was decreased by 62% (from 8.47 to 3.22 nm) via FLA, while inhibiting the leakage current that limit current efficiency (CE) of perovskite LED (PeLED). Three dimensional temperature simulation was investigated for the mechanism of flash-induced $MAPbBr_3$ recrystallization. Finally, FLA was successfully exploited for the flexible PeLEDs on polyethylene naphthalate substrates, which exhibited 252% larger CE compared to thermally annealed counterpart.

1. Introduction

According to the Shockley-Queisser limit, recent dramatic advance of organic–inorganic halide perovskite (OIHP) solar cell (power conversion efficiency improvement by 23.3% within just six years) suggests a significant potential of hybrid perovskites also in luminescent applications, such as laser and light-emitting diode (LED) [1–3]. Contradictory features of the organic and inorganic elements in OIHP are synergistically integrated to realize excellent material properties (e.g., carrier mobility and lifetime, quantum efficiency, color purity and flexibility) as well as chromatic tunability and solution processability [4–6]. Consequently, OIHPs are emerging as promising materials that can complement conventional organic LED (OLED) [7]. Unfortunately, perovskite LEDs (PeLED) still suffer from poor luminescence efficiencies along with the high surface roughness (leakage current), large grain size (exciton dissociation) and defect formation (non-radiative recombination) in the OIHP active layer, which are generally caused by a crude self-assembly process relying on solution coating [8–10]. Extensive research efforts have been devoted to address the aforementioned issues by various approaches, including nanocrystal pinning (NCP), OIHP coarsening, trap site passivating and polymer mixing [8,11–15]. Nonetheless, coarsening of the organometal halide perovskites readily results in non-uniform and large cuboid crystals, while forming numerous voids and pinholes in the layer that cause leakage current of a device [16]. Incorporating a dielectric polymer matrix or passivation additives into a hybrid perovskite can deteriorate series conductance and charge transport characteristics of PeLEDs, respectively [11]. Notably, Cho et al. recently demonstrated a densely covered, tiny grain (ranging from 50 to 150 nm) OIHP film by an NCP method [8]. This approach is highly successful in the enhancement of PeLED efficiency but large-area uniform solution process still remains a practical challenge.

Light–material interaction (e.g., low temperature polycrystalline silicon (LTPS)) is attracting a great deal of research attention as a powerful generalized pathway towards the well-defined control of grain boundary interface formation and crystal growth of various functional

* Corresponding author.
** Corresponding author.
E-mail addresses: keonlee@kaist.ac.kr (K.J. Lee), sangouk@kaist.ac.kr (S.O. Kim).
[1] These authors equally contributed to this work.

https://doi.org/10.1016/j.nanoen.2019.04.061
Received 15 March 2019; Received in revised form 13 April 2019; Accepted 17 April 2019
Available online 20 April 2019

materials [17–21]. Its genuine capability to stimulate the none-quilibrium photon reactions within extremely confined region and time span can trigger damage-free thermal response of heat-sensitive matter (e.g., OIHP and polymer), which is hardly attainable under traditional thermal heating process [22–26]. From the perspective for an inexpensive and scalable light source, xenon flash lamps have been spotlighted together with their rapid (from μs to ms) and large-scale processability, high light output efficiency and genuine compatibility to roll-to-roll process [27–30]. Noteworthy that a concept of flash light annealing (FLA) has yet been fundamentally restricted to PeLED application primarily due to the concerns for the radiative damage from intrinsic ultraviolet (UV) of broad wavelength spectrum (invasive to OIHP) and difficulties of governing perovskite grain growth [31].

Herein, we report the first FLA recrystallization of perovskite crystal structure (methylammonium lead tribromide, $MAPbBr_3$), particularly aiming at LEDs. Intense NIR peak spectral lines of flash light were generated by discharging a lamp at low current density, which were selectively transmitted thorough UV-filtering glass (borosilicate coated) to minimize the UV degradation of perovskite. Despite the low NIR absorption of $MAPbBr_3$, intensive heat was generated from the underneath charge transport layer consisting of poly (3,4-ethylenedioxythiophene) polystyrene sulfonate (PEDOT:PSS) and indium tin oxide (ITO). Flash-activated ultrafast heating and quenching (within milisecond) could realize the recrystallization of NCP-based cuboid $MAPbBr_3$ crystal in a precisely controlled manner without noticeable radiative damage even in a harsh thermal stress over ~320 °C, enabling dense perovskite film with exceptionally small grain size (~38 nm). To the best of our knowledge, this noticeable grain size enabled by FLA is smallest compared to the previously reported perovskite films and thereby effectively enhances the spatial confinement effect of excitons.

2. Experimental section

Photothermal simulation: For the simulation of photothermal annealing mechanism by FLA process, FEA simulation was performed. The thermal flux simulation was carried out by the COMSOL Multiphysics 5.3 software using the heat transfer mode. Perovskite cuboidal nanograin structure (~62 nm size) was modeled by using random distribution mode in the simulation program [32]. During rapid flash irradiation, thermal distribution within PeLED structure was calculated by a heat transfer equation. The entire PeLED structure was constructed while considering the film thickness of ITO (150 nm), PEDOT:PSS (50 nm) and $MAPbBr_3$ (160 nm). Furthermore, The density, thermal capacity, thermal conductivity, molecular weight, and absorption coefficient of $MAPbBr_3$ layer was 3.83 g cm^{-3} [33], 170 J $K^{-1}mol^{-1}$ [34], 0.51 W $m^{-1}K^{-1}$, [32] 0.39 W $m^{-1}K^{-1}$ [35], 479 g mol^{-1} [33] and 10^{-2} cm^{-1} [36], respectively.

Device fabrication: An ITO coated glass substrate (corning glass, 20 Ω·sq^{-1}) was cleaned with the deionized water, aceton and 2-isopropanol for 15 min using ultrasonication bath. The PEDOT:PSS (AI 4083, Clevios PVP) solution was spin-coated at 4000 rpm for 50 s on the UV-ozone treated ITO substrate and annealed at the 150 °C for 15 min. To prepare the perovskite precursor solution (30 wt%), methylammonium bromide (MABr, Dyesol, purity > 98%) and lead (II) bromide ($PbBr_2$, Sigma Aldrich, purity > 99.999%) were mixed into 1.05:1 M ratio and dissolved into co-solvent of γ-butyrolacton (GBL, Sigma Aldrich)/dimethylsulfoxide (DMSO, Sigma Aldrich) with 7:3 vol ratio. The precusor was spin-coated on the PEDOT:PSS layer at 3000 rpm for 55 s in the glove box filled with N_2. During spin coating, the 30 μl of chlorobenzene/chloroform (1:1 v/v) co-solvent with 0.1 wt% bathocuproine (BCP, Sigma Aldrich, purity > 99.999%) was dropped on the perovskite precursor to make uniform film. The flash light was irradiated on the spin-coated perovskite film under ambient condition during 660 μs for rapid annealing induced by strong photothermal conversion. BCP dissolved in chlorobenzene (8 mg/ml) was spin-coated at 5000 rpm for 45 s in a globe box and annealed at 90 °C for 5 min. Finally, the LiF (1 nm)/Al (80 nm) were sequentially deposited under the high vacuum (≈ 3×10^{-6} torr) to form electrode using thermal evaporation system. The active area of PeLED was 18 mm^2 (9 mm × 2 mm).

Characterizations: The morphologies and crystalline structure of the $MAPbBr_3$ films were characterized by means of SEM (S-4800, Hitachi), AFM (SPA-400, Seiko instrument) and XRD (D/MAX-2500, Rigaku). The chemical and elemental compositions of the perovskite layers were monitored with XPS (K-Alpha, Thermo VG Scientific). The photoluminescence properties of perovskites were analyzed by various measurement systems. Steady state PL was obtained by Raman/Photoluminescence spectroscopy (LabRAM HR UV/Vis/NIR, HORIBA Jobin Yvon Inc.). Time-resolved PL of perovskite was observed by time-correlated single-photon counting system (iHR320, HORIBA Jobin Yvon Inc.). The temperature dependent PL spectra was measured by Dispersive raman spectrometer (ARAMIS, HORIBA Jobin Yvon Inc.). Absorption spectra of perovskite layer was observed by UV-vis spectrometer (SolidSpec-3700, Shimadzu). The current-voltage-luminance characteristics and device efficiency were measured by Keithely 2400 source measurement system and spectroradiometer (SR-3A, Topcon).

3. Results and discussion

Fig. 1 schematically illustrates the overall concept of FLA for ultrafast recrystallization of perovskite material. $MAPbBr_3$ solution was spin-coated on the glass/ITO/PEDOT:PSS substrates by additive NCP method. The formulated pervoskite crystal layer had a rough surface and lots of voids due to the cuboidal morphology. A xenon flash lamp sealed by a borosilicate glass was utilized to filter the UV flash spectrum, which can induce a specific bond dissociation of the OIHP material [31]. The strong line radiation of xenon flash lamp in the NIR regime propogated through the $MAPbBr_3$ and induced the photothermal effect particularly at PEDOT:PSS and ITO charge transport layer, triggering a melting of the perovskite without photothermal damage (Fig. 1a–ii). As described in Fig. 1a–iii, an immediate recrystallization of $MAPbBr_3$ was induced under the ultrafast annealing and effectively transformed the cuboid perovskite structure into densely recrystallized OIHP film with fine grains and smooth surface.

Due to the difficulties of direct measurement of the perovskite temperature during FLA, FEA calculation was carried out for a reliable verification of the flash-induced $MAPbBr_3$ phase transformation, as presented in Fig. 1b. For a reliable verification of the $MAPbBr_3$ phase transformation, FEA calculation was carried out, as presented in Fig. 1b. The temperature of the glass/ITO/PEDOT:PSS/$MAPbBr_3$ structure during FLA process was simulated by the following heat flux equation (1) [37,38].

$$Q = \rho C \frac{\partial T}{\partial t} + \rho C \cdot \nabla T - \nabla \cdot (k \nabla T) \quad (1)$$

where Q is the total thermal energy generated by the flash light irradiation and ρ, C and k are the density, heat capacity and thermal conductivity of the $MAPbBr_3$, PEDOT:PSS, ITO and glass, respectively. Monochromatic plane wave (wavelength of 900 nm) was applied for the simulation to consider the spectrum of flash light with the highest peak intensity at 900 nm wavelength (Fig. S1, Supporting Information). The flash light (660 μs pulse width) with various energy densities from 3.3 to 6.1 J cm^{-2} was utilized to calculate the FLA effect within the model perovskite architecture (more detailed procedures are indicated in experimental section). As depicted in Fig. 1b, the photothermal heating was preferentially nucleated from the high light absorbing layers of PEDOT:PSS and ITO with the energy density of 4 J cm^{-2}. Noteworthy that flash light is unable to directly excite an effective photothermal effect in the $MAPbBr_3$ film due to the low absorption coefficient in the NIR spectral region (Fig. S3, Supporting Information). By contrast, free charge carriers in the PEDOT:PSS and ITO could synergistically absorb the intense NIR of flash light and transfer the thermal energy to the

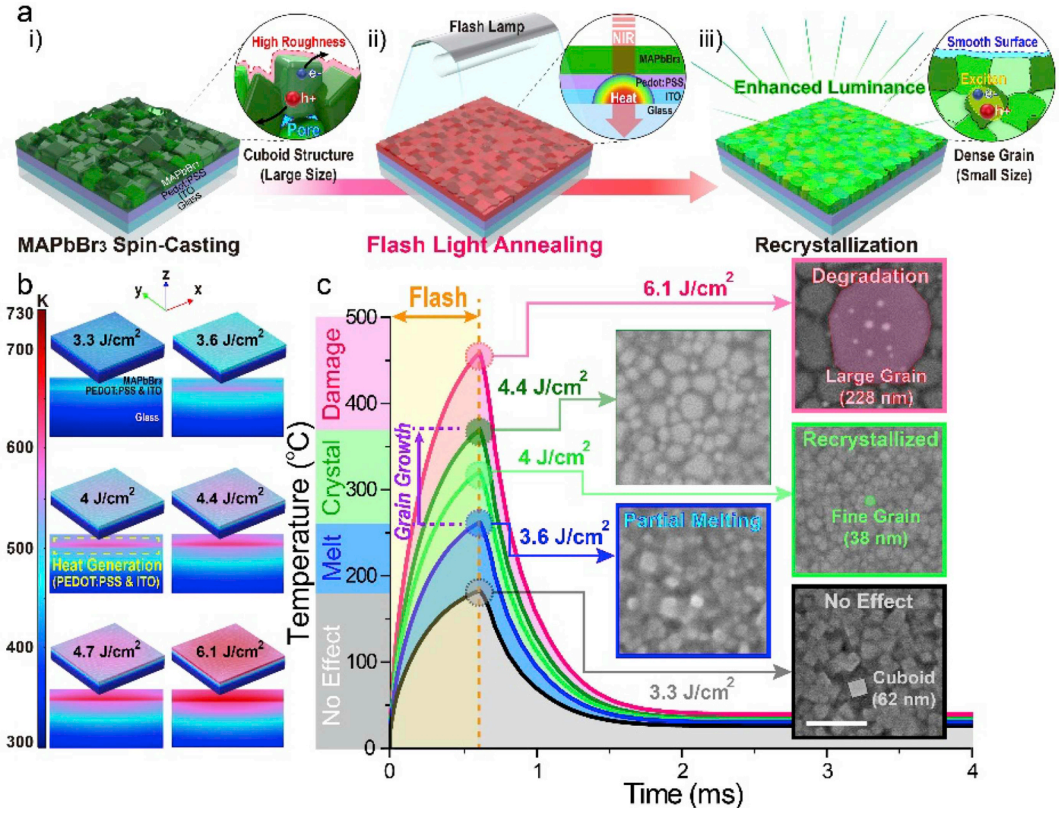

Fig. 1. a) Schematic illustrations of the flash-induced ultrafast recrystallization of perovskite ($MAPbBr_3$). b) FEA calculation for the temperature distribution of the glass/ITO/PEDOT:PSS/$MAPbBr_3$ under flash light irradiation (660 μs pulse width) with energy densities from 3.3 to 6.1 J cm^{-2}. c) Simulated surface temperature and experimentally evolved morphology (SEM image) of the perovskite under various flash light irradiation condition (at pulse width of 660 μs and energy densities from 3.3 to 6.1 J cm^{-2}). White scale bar is 250 nm.

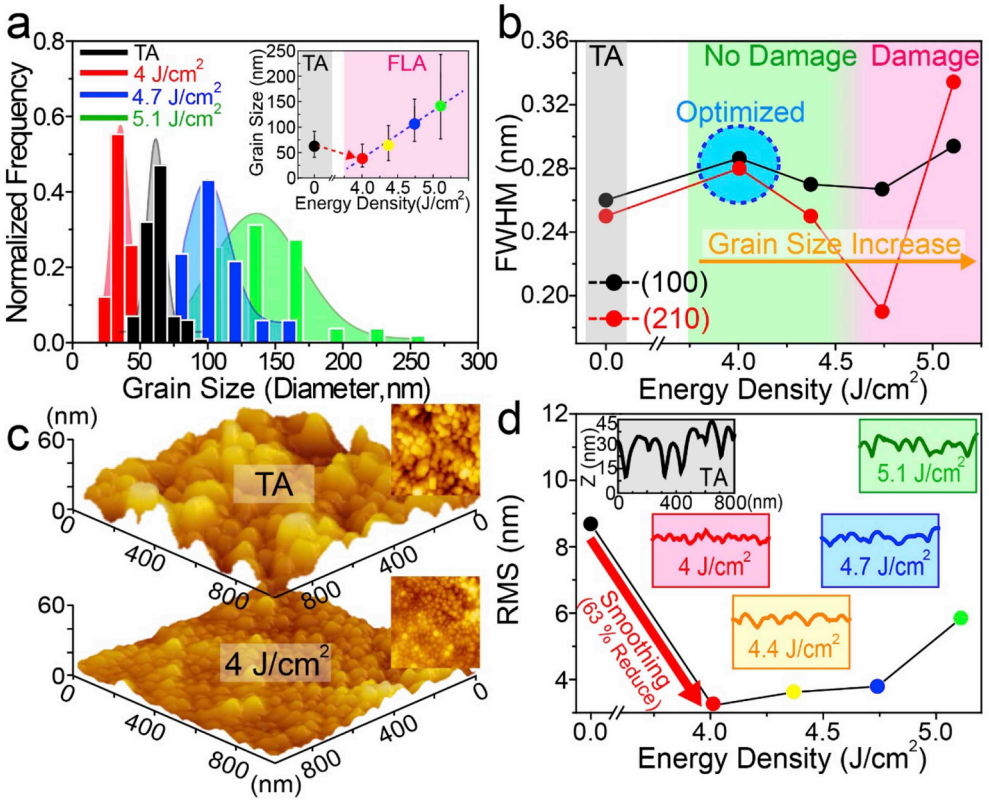

Fig. 2. a) Grain size distribution of perovskites processed by TA and FLA. Inset of Fig. 2a shows average grain size of $MAPbBr_3$ films annealed by conventional static heating and flash light irradiation. b) XRD FWHM of the TA and FLA-induced perovskites. c) 3D surface morphology of the $MAPbBr_3$ layers treated by TA and FLA (4 J cm^{-2}). Insets present plane view AFM image of the corresponding OIHP films. d) RMS of the thermally annealed and flash-induced perovskites measured by AFM. Insets illustrate the line AFM profiles of the surface of the perovskites demonstrated via TA and different FLA condition.

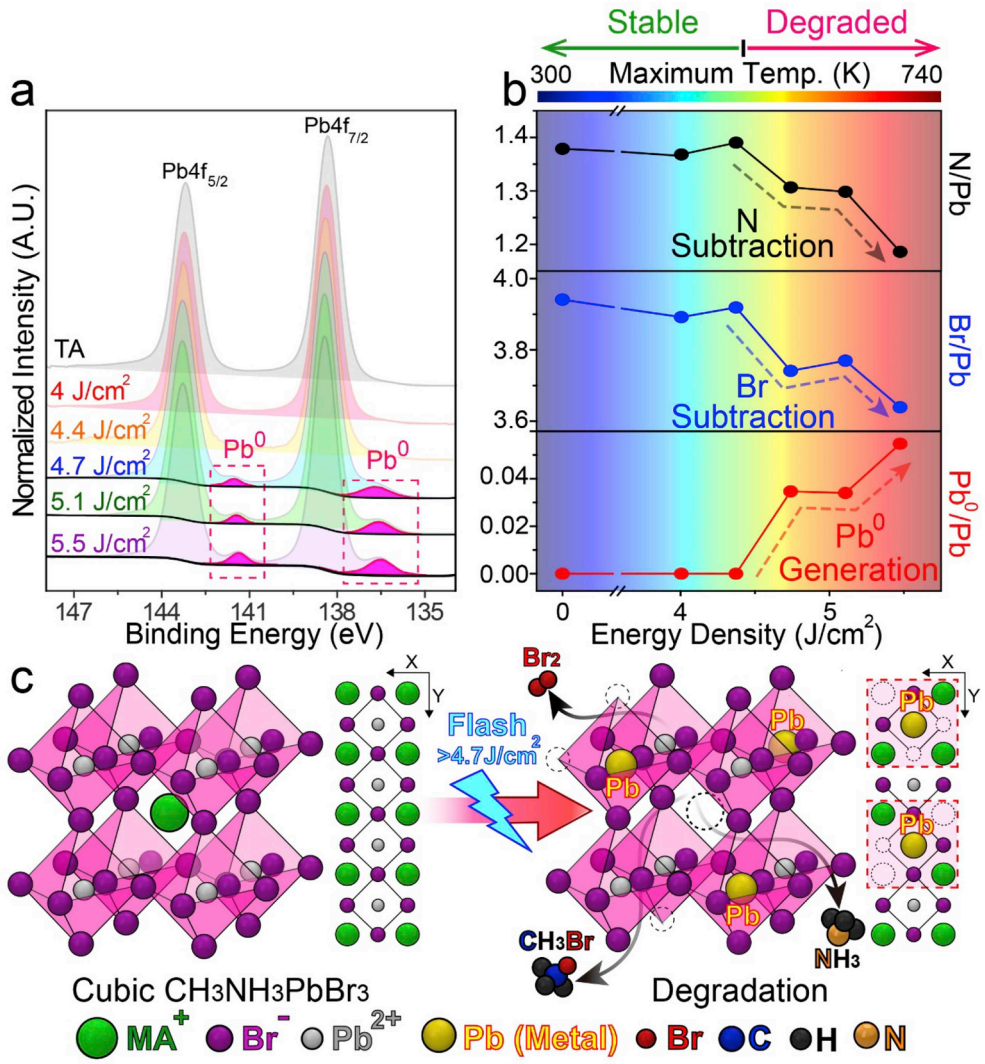

Fig. 3. a) Normalized intensity of XPS for the perovskite samples under TA and FLA. b) Relative atomic ratio of N, Br and Pb^0 to total Pb measured by XPS. c) Schematic $MAPbBr_3$ degradation model caused by harsh flash light processing.

$MAPbBr_3$ in the form of phonon vibration, as experimentally confirmed in Fig. S4 (Supporting Information) [24]. The simulated flash-induced temperature of the top perovskite surface reached up to 730 K (at 6.1 J cm^{-2}), exhibiting a sufficient thermal energy for the melting and recrystallization of $MAPbBr_3$. The stability of PEDOT:PSS at high temperature during FLA was also confirmed by raman spectra, as shown in Fig. S5.

Fig. 1c compares the calculated surface temperature and experimentally observed morphology of perovskite film with various energy densities from 3.3 to 6.1 J cm^{-2} (pulse width of 660 μs). Under the FLA of 3.3 J cm^{-2}, no significant photothermal effect was induced, thus remaining the original cuboid structure. The OIHP layer began to demonstrate a partial melting at 3.6 J cm^{-2} energy density without solid-state cuboidal grain growth, indicating that ~260 °C is a threshold temperature. At 4 J cm^{-2} flash light energy density, morphology of the cuboidal perovskite film was completely transformed into a recrystallized phase with uniform close packed grains with remarkably small size (~38 nm), which can only occur by melting and recrystallization [39]. This reduced grain size, and intense densification of perovskite film can be beneficial for the spatial confinement of excitons within tiny $MAPbBr_3$ grains, and the reduction of trap sites respectively, both of which are desirable for the effective enhancement of radiative exciton recombination [8,40,41]. The recrystallization of OIHP materials has been regarded difficult to attain, since these hybrid materials with organic component can be easily decomposed before reaching the melting temperature [42]. Nonetheless, we succeeded in the effective recrystallization of $MAPbBr_3$ without degradation by ultrafast FLA process particularly under ambient atmosphere. Over 4.4 J cm^{-2}, grain size of $MAPbBr_3$ was increased as illustrated in the SEM images of Fig. 1c. When an excessive flash light (energy density of 6.1 J cm^{-2}) was exposed to $MAPbBr_3$, severe photothermal damage was observed in the perovskite layer (Fig. S4-iv, Supporting Information). Noteworthy that an equivalent recrystallization effect was observed by a flash light with longer pulse duration (3.6 ms), however, noticeable degradation was caused in the perovskite layer under the extended processing time (Fig. S6, Supporting Information).

Fig. 2a compares the statistical size distributions of perovskite grains induced by traditional thermal annealing (TA) and FLA (energy density from 4 to 5.1 J cm^{-2}). The average grain size of $MAPbBr_3$ induced by the energy density of 4 J cm^{-2} was ~38 nm, presenting 39% reduction compared to that of cuboid OIHP film treated by TA. Noteworthy that this grain size corresponds the smallest value ever reported thus far. As the flash light energy density gradually increased to 5.1 J cm^{-2}, the average grain size proportionally increased to 141.4 nm (inset of Fig. 2a). Fig. 2b compares the full width half maximum (FWHM) of (100) and (210) X-ray Diffraction (XRD) peaks of $MAPbBr_3$ processed via TA and FLA. The FWHM of 4 J cm^{-2} flash treated $MAPbBr_3$ is higher than those from TA treated counterpart. FWHM is

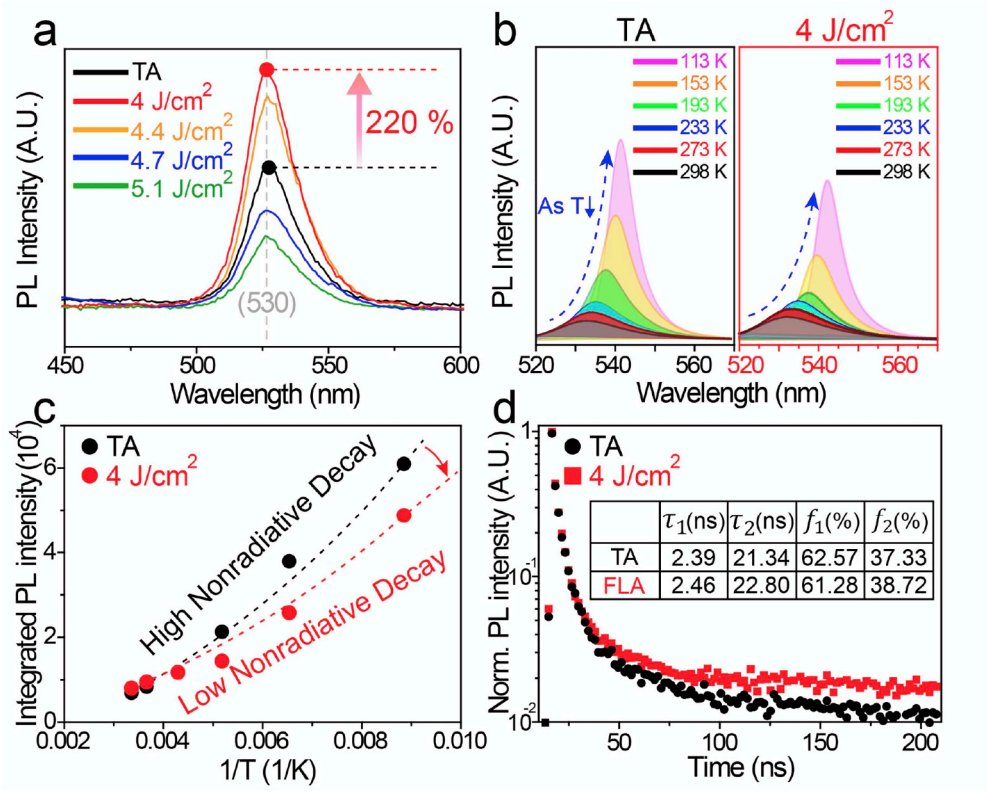

Fig. 4. a) PL intensity of the TA and FLA-induced perovskite films. b) PL intensity of the $MAPbBr_3$ processed by TA and FLA at 4 J cm^{-2} under various temperature from 298 to 113 K. c) Integrated PL intensity of the OIHP layers (TA and FLA at 4 J cm^{-2}) as a function of temperature. d) Normalized PL intensity of the $MAPbBr_3$ treated by TA and FLA at 4 J cm^{-2}. Inset indicates the carrier lifetime of the thermally annealed and flash-induced (4 J cm^{-2}) perovskites measured by TRPL measurement.

known to become higher along with the reduction of grain size [43,44]. Moreover, as the FLA energy density increased from 4.4 to 4.7 J cm^{-2}, the FWHM gradually decreased, which is mainly attributed to the size enlargement of $MAPbBr_3$ grain induced by harsh FLA process. In spite of the gradual grain size increase at 5.1 J cm^{-2}, FWHM increased because of significantly diminished crystallinity caused by serious photothermal-decomposition of $MAPbBr_3$.

Fig. 2c ellucidates the surface morphology of the perovskite film treated by TA and FLA (4 J cm^{-2}), measured via an atomic force microscopy (AFM). The FLA-induced OIHP exhibited a smooth surface layer, while the original cuboid $MAPbBr_3$ layer presented high roughness with numerous voids. As shown in Fig. 2d, surface roughness (RMS) of the perovskite demonstrated by FLA at 4 J cm^{-2} is 63% lower value than that of TA-induced counterpart. The hole blocking layer (BCP, thickness of ~50 nm) coated on this low roughness film can prevent the direct contact (leakage path) between the perovskite layer and cathode [45].Along with the energy density increase from 4.4 to 5.1 J cm^{-2}, RMS of perovskite layer also became gradually increased.

For the identification of any radiative damage effect by FLA on the perovskite layer, X-ray photoelectron spectroscopy (XPS) analysis was performed (Fig. 3a). The XPS spectra of the flash-induced perovskite film (at 4 and 4.4 J cm^{-2}) presented typical $MAPbBr_3$ crystalline peaks ($Pb4f_{5/2}$ and $Pb4f_{7/2}$) without any evidence for radiative damage. By contrast, Pb^{2+} ions present in the center of $MAPbBr_3$ got reduced to metallic lead (Pb^0) by a flash light over 4.7 J cm^{-2}. Fig. 3b shows the relative atomic ratio of $MAPbBr_3$ components (N, Br, Pb^0) to total Pb. The atomic ratios of N/Pb, Br/Pb and Pb^0/Pb maintained constant levels below 4.4 J cm^{-2} energy density, above which the N/Pb and Br/Pb suddenly decreased, whereas Pb^0/Pb increased. This indicates that the N and Br components in $MAPbBr_3$ crystals were eliminated together with the light-induced reduction of Pb^0, resulting in the disorientation of OIHP crystallinity. Interestingly, this flash-induced $MAPbBr_3$ degradation mechanism could be supported by following chemical formula, which thermodynamically yields CH_3Br, NH_3 and Br_2 gas products from MA cations [46].

$$CH_3NH_3PbBr_3\ (s) \rightarrow CH_3Br\ (g)\uparrow + NH_3\ (g)\uparrow + Br_2\ (g)\uparrow + Pb^0$$

Fig. 3c schematically illustrates the degradation mechanism. According to the proposed mechanism, the undesired by-products including Pb^0 metal, and CH_3Br, NH_3 and Br_2 gases, create numerous exciton quenching and non-radiative decay sites. Furthermore, we degraded the thermal annealed and flash light annealed $MAPbBr_3$ films by storing them at 25 °C in humid condition (RH > 70%) for 2 days to characterize their stability. The FLA-induced perovskite showed reasonable stability which is comparable to that of the TA-treated $MAPbBr_3$, as represented at Fig. S7.

Fig. 4a presents the photoluminescence (PL) properties of the $MAPbBr_3$ films processed by TA and FLA. The peak positions of PL were located at ~530 nm with narrow FWHM of ~21 nm (FWHM of organic emitters > 40 nm) [47]. PL of the film prepared by 4 J cm^{-2} flash light presented 220% higher value than thermally annealed one. Obviously, this enhancement is ascribed to the dense/flat film morphology as well as small grain size (exciton confinement effect) of FLA induced perovskite layer. At a higher density of 4.4 J cm^{-2}, the PL intensity is lower with the larger crystalline grain size of $MAPbBr_3$. When the FLA is over 4.7 J cm^{-2}, PL is significantly deteriorated presumably accompanied with the strong quenching effect from Pb^0 atoms and decomposition of the $MAPbBr_3$.

Temperature-dependent PL measurements were carried out for the perovskite layers prepared by TA and 4 J cm^{-2} FLA to compare charge trap densities that may cause non-radiative decay (Fig. 4b). In general, PL of the perovskites with a large amounts of non-radiative decay channels is intensified at a low temperature, while thermal disturbance (via the trap sites) of radiative decay can be greatly reduced [48]. The measurement temperature was varied from 298 to 113 K (40 K increment) during the steady-state PL measurements. Fig. 4c presents the integrated PL intensity vs. environmental temperature for TA and FLA (4 J cm^{-2}). Upon the cooling down to 113 K, TA treated perovskite layer revealed a higher increase of the integrated PL than FLA treated counterpart. This verifies that non-radiative decay in OIHP could be greatly reduced by FLA treatment. In addition, we performed the time-

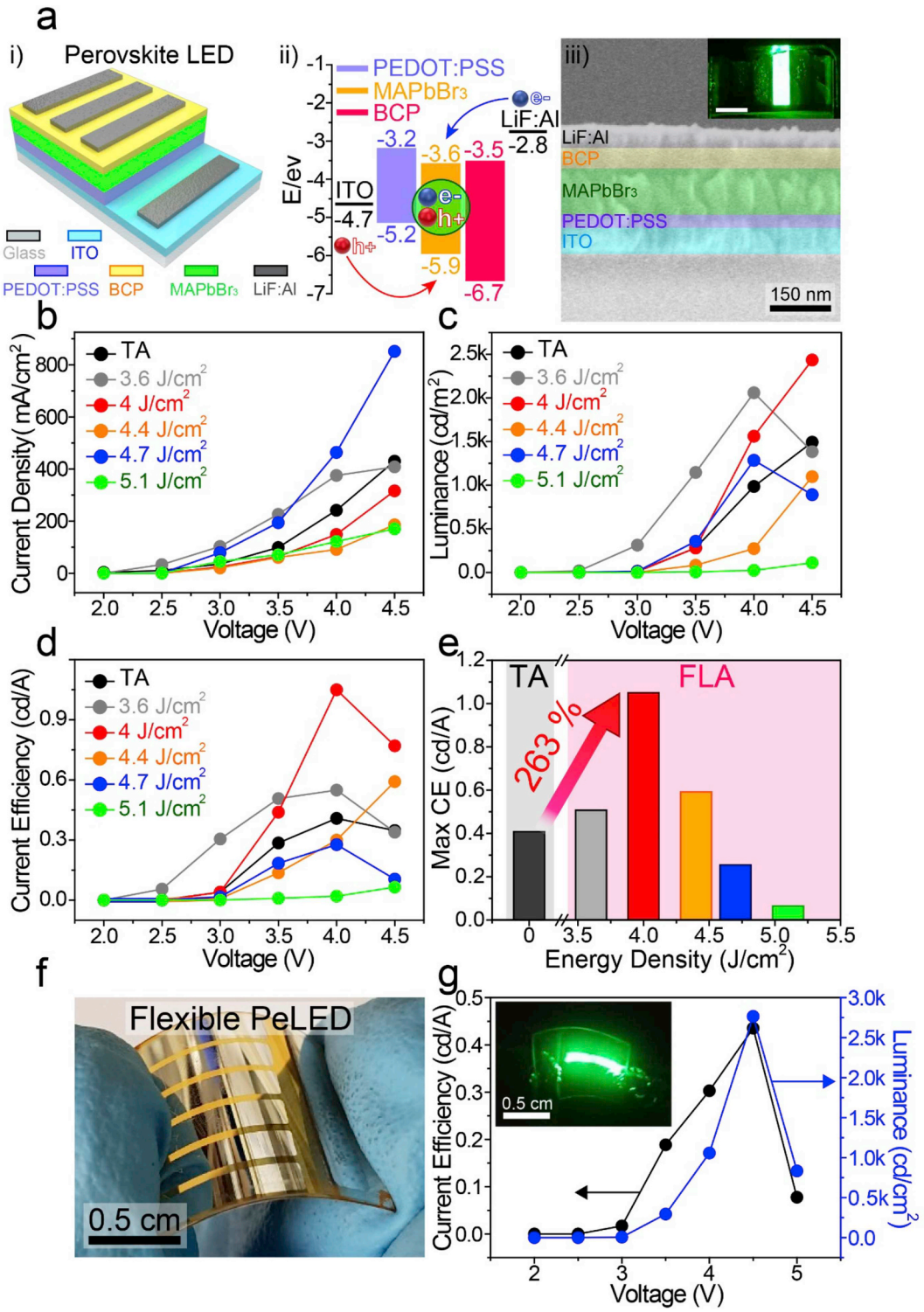

Fig. 5. a-i) Schematic illustration of PeLED device. a-ii) Energy level diagram of PeLED layers (with respect to vacuum). a-iii) Cross section SEM image of a PeLED. b-d) Device performances of the PeLED devices (current density, luminance and current efficiency as a function of voltage) fabricated by TA and various FLA condition from 3.6 J cm^{-2} to 5.1 J cm^{-2}. e) Maximum current efficiencies of the PeLEDs based on thermally annealed and flash-induced $MAPbBr_3$. f) Photographic image of flexible PeLED on PEN plastic. g) Current efficiency and luminance of flexible PeLED demonstrated by flash light irradiation.

resolved PL (TRPL) measurements for the samples prepared by TA and FLA (4 J cm^{-2}), as shown in Fig. 4d. Both shorter (τ_1) and longer (τ_2) lifetimes of OIHP carriers were extended by FLA, resulting in 9.3% increment of average carrier lifetime (from 9.46 to 10.34 ns) (Table S3). This improved carrier lifetime is realized by the successful suppression of exciton dissociation and charge trap site formation by our optimal FLA treatment.

To clarify the advantageous effect from FLA on PeLED performance, we fabricated the LEDs based on the $MAPbBr_3$ films treated by TA and FLA. Fig. 5a–i and 5a-ii schematically depict the device architecture and energy level of the PeLED. ITO anode (150 nm), PEDOT:PSS (50 nm) hole injection/transport layer and $MAPbBr_3$ (150 nm) were sequentially deposited on a glass substrate, which was followed by either TA or FLA. Afterwards, BCP (50 nm) and LiF (1 nm):Al (80 nm) were formed as ETL

layer and cathode, respectively. As presented in the SEM image of Fig. 5a–iii, smooth device layers were well-formed without pores and leakage paths. Fig. 5b–d shows the current density, luminescence and current efficiency curves of the PeLEDs as a function of applied voltage potential. The current efficiency of PeLED device processed by TA and FLA (3.6, 4, 4.4 J cm^{-2}) decreased at the high bias condition due to the loss of carrier recombination, which is a commonly observable phenomena [49,50]. A maximum brightness of 2434 cd m^{-2} was achieved at the current density of 316 mA cm^{-2} for the PeLED processed by the optimized FLA (4 J cm^{-2}) (Fig. 5b and c). Moreover, as indicated in Fig. 5e, the 4 J cm^{-2} FLA-induced PeLED demonstrated the highest maximum current efficiency (CE) of 1.05 cd/A, exhibiting 2.6 times higher value than that of TA-induced device (0.40 cd/A). The maximum CE continuously decreased with the further increase of flash light intensity due to the undesired side effects from excessive FLA processing, including enlargement of crystalline grain size and photodegradation. Noteworthy that the CE can be improved with a further effort for device optimization, such as perovskite film thickness and ETL material choice (mobility, charge carrier balance).

To present the practical feasibility of FLA process for flexible device application, FLA-induced PeLED was implemented on a heat-sensitive polyethylene naphthalate (PEN) substrate, as illustrated in Fig. 5f. Noteworthy that our instantaneous ultrafast photothermal FLA process enabled a stable recrystallization of the perovskite layer without thermal damage upon the PEN with a moderate melting temperature around 250 °C.[41] Moreover, despite the relatively rough surface of commercially available PEN substate and conventional quality ITO film (moderate conductance), our flexible PeLED prepared by FLA showed a reasonable performance with 252% higher CE and 409% brighter luminance than TA-induced counterpart (Fig. 5g and Fig. S12, Supporting Information). In addition, these results can also be extended to the stability optimization of the flash-induced PeLED device, which will be a crucial technology to resolve key issue of current perovskite research field. Obviously, the processing speed of FLA (660 μs) is far faster than that of conventional TA, enabling a rapid and continuous crystallization of OIHP film over the large area plastic film, offering a intrinsic potential for the process compatibility with flexible PeLED mass production.

4. Conclusion

We have demonstrated ultrafast recrystallization of optoelectronic OIHP perovskite film via FLA. Strong NIR peaks (830 and 900 nm) from UV filtered FLA could effectively recrystallize the OIHP layer without radiative degradation. 3D simulations successfully verified the melting and recrystallization mechanism based on our ultrafast photothermal process. Dense and uniform highly crystalline $MAPbBr_3$ film could be readily obtained with a remarkably small grain size down to ~38 nm. Flexible PeLEDs as well as typical rigid devices were successfully fabricated by FLA, exhibiting 2.5 times higher CE than the TA induced counterpart on commercial PEN substrate. This work manifests the unprecedented potential of FLA for the highly functional complex materials even including organic component, which is generally weak for high energy radiation, by means of delicate controllability of processing conditions, such as radiative wavelength distribution and processing temperature/time. The fundamental lessons from this work propose valuable opportunities for the scalable large area production of various organic-inorganic hybrid based structures and devices, including flexible solar cells, wearable photodetectors and lasers on plastic.

Acknowledgments

D.H.J. and J.H.P. contributed equally to this work. This work was supported by the National Creative Research Initiative (CRI) Center for Multi-Dimensional Directed Nanoscale Assembly (2015R1A3A2033061) and the Global Frontier Hybrid Interface Materials (GFHIM) of the National Creative Research Initiative (CRI) Center for Multi-Dimensional Directed Nanoscale Assembly (2013M3A6B1078874). K.J.L. is thankful to the Creative Materials Discovery Program through the National Research Foundation of Korea (NRF) funded by the Ministry of Science and ICT (2016M3D1A1900035) and the Nano Material Technology Development Program through the NRF funded by the Ministry of Science, ICT and Future Planning (2016M3A7B4905621).

Appendix A. Supplementary data

Supplementary data to this article can be found online at https://doi.org/10.1016/j.nanoen.2019.04.061.

References

[1] S.D. Stranks, H.J. Snaith, Nanotechnology 10 (2015) 391.
[2] T.A. Berhe, W.-N. Su, C.-H. Chen, C.-J. Pan, J.-H. Cheng, H.-M. Chen, M.-C. Tsai, L.-Y. Chen, A.A. Dubale, B.-J. Hwang, Energy Environ. Sci. 9 (2016) 323.
[3] X. Xiao, C. Bao, Y. Fang, J. Dai, B.R. Ecker, C. Wang, Y. Lin, S. Tang, Y. Liu, Y. Deng, X. Zheng, Y. Gao, X.C. Zeng, J. Huang, Nat. Commun. 30 (2018) 1705176.
[4] Y. Cao, N. Wang, H. Tian, J. Guo, Y. Wei, H. Chen, Y. Miao, W. Zou, K. Pan, Y. He, H. Cao, Y. Ke, M. Xu, Y. Wang, M. Yang, K. Du, Z. Fu, D. Kong, D. Dai, Y. Jin, G. Li, H. Li, Q. Peng, J. Wang, W. Huang, Nature 562 (2018) 249.
[5] Y.-H. Kim, H. Cho, J.H. Heo, T.-S. Kim, N. Myoung, C.-L. Lee, S.H. Im, T.-W. Lee, Adv. Mater. 27 (2015) 1248.
[6] Z.-K. Tan, R.S. Moghaddam, M.L. Lai, P. Docampo, R. Higler, F. Deschler, M. Price, A. Sadhanala, L.M. Pazos, D. Credgington, F. Hanusch, T. Bein, H.J. Snaith, R.H. Friend, Nat. Nanotechnol. 9 (2014) 687.
[7] Y.-H. Kim, H. Cho, T.-W. Lee, Proc. Natl. Acad. Sci. U.S.A. 113 (2016) 11694.
[8] H. Cho, S.-H. Jeong, M.-H. Park, Y.-H. Kim, C. Wolf, C.-L. Lee, J.H. Heo, A. Sadhanala, N. Myoung, S. Yoo, S.H. Im, R.H. Friend, T.-W. Lee, Science 350 (2015) 1222.
[9] A. Buin, R. Comin, J. Xu, A.H. Ip, E.H. Sargent, Chem. Mater. 27 (2015) 4405.
[10] F. Jin, B. Zhao, B. Chu, H. Zhao, Z. Su, W. Li, F. Zhu, J. Mater. Chem. 6 (2018) 1573.
[11] G. Li, Z.-K. Tan, D. Di, M.L. Lai, L. Jiang, J.H.-W. Lim, R.H. Friend, N.C. Greenham, Nano Lett. 15 (2015) 2640.
[12] M. Abdi-Jalebi, Z. Andaji-Garmaroudi, S. Cacovich, C. Stavrakas, B. Philippe, J.M. Richter, M. Alsari, E.P. Booker, E.M. Hutter, A.J. Pearson, S. Lilliu, T.J. Savenije, H. Rensmo, G. Divitini, C. Ducati, R.H. Friend, S.D. Stranks, Nature 555 (2018) 497.
[13] X. Yang, X. Zhang, J. Deng, Z. Chu, Q. Jiang, J. Meng, P. Wang, L. Zhang, Z. Yin, J. You, Nat. Commun. 9 (2018) 570.
[14] J. Li, S.G.R. Bade, X. Shan, Z. Yu, Adv. Mater. 27 (2015) 5196.
[15] T. Jeon, S.J. Kim, J. Yoon, J. Byun, H.R. Hong, T.-W. Lee, J.-S. Kim, B. Shin, S.O. Kim, Adv. Energy Mater. 7 (2017) 1602596.
[16] Y.-K. Chih, J.-C. Wang, R.-T. Yang, C.-C. Liu, Y.-C. Chang, Y.-S. Fu, W.-C. Lai, P. Chen, T.-C. Wen, Y.-C. Huang, C.-S. Tsao, T.-F. Guo, Adv. Mater. 28 (2016) 8687.
[17] D.J. Joe, S. Kim, J.H. Park, D.Y. Park, H.E. Lee, T.H. Im, I. Choi, R.S. Ruoff, K.J. Lee, Adv. Mater. 29 (2017) 1606586.
[18] H. Palneedi, J.H. Park, D. Maurya, M. Peddigari, G.-T. Hwang, V. Annapureddy, J.-W. Kim, J.-J. Choi, B.-D. Hahn, S. Priya, K.J. Lee, J. Ryu, Adv. Mater. 30 (2018) 1705148.
[19] J.H. Park, S. Han, D. Kim, B.K. You, D.J. Joe, S. Hong, J. Seo, J. Kwon, C.K. Jeong, H.-J. Park, T.-S. Kim, S.H. Ko, K.J. Lee, Adv. Funct. Mater. 27 (2017) 1701138.
[20] J.H. Park, S. Jeong, E.J. Lee, S.S. Lee, J.Y. Seok, M. Yang, Y. Choi, B. Kang, Chem. Mater. 28 (2016) 4151.
[21] T. Shimoda, Y. Matsuki, M. Furusawa, T. Aoki, I. Yudasaka, H. Tanaka, H. Iwasawa, D. Wang, M. Miyasaka, Y. Takeuchi, Nature 440 (2006) 783.
[22] M.F. El-Kady, V. Strong, S. Dubin, R.B. Kaner, Science 335 (2012) 1326.
[23] E.C. Garnett, W. Cai, J.J. Cha, F. Mahmood, S.T. Connor, M. Greyson Christoforo, Y. Cui, M.D. McGehee, M.L. Brongersma, Nat. Mater. 11 (2012) 241.
[24] T. Jeon, H.M. Jin, S.H. Lee, J.M. Lee, H.I. Park, M.K. Kim, K.J. Lee, B. Shin, S.O. Kim, ACS Nano 10 (2016) 7907.
[25] H.M. Jin, S.H. Lee, J.Y. Kim, S.-W. Son, B.H. Kim, H.K. Lee, J.H. Mun, S.K. Cha, J.S. Kim, P.F. Nealey, K.J. Lee, S.O. Kim, ACS Nano 10 (2016) 3435.
[26] J.H. Park, J. Seo, C. Kim, D.J. Joe, H.E. Lee, T.H. Im, J.Y. Seok, C.K. Jeong, B.S. Ma, H.K. Park, T.-S. Kim, K.J. Lee, Adv. Sci. 5 (2018) 1801146.
[27] D. Angmo, T.T. Larsen-Olsen, M. Jørgensen, R.R. Søndergaard, F.C. Krebs, Adv. Energy Mater. 3 (2013) 172.
[28] T.H. Im, D.Y. Park, H.K. Lee, J.H. Park, C.K. Jeong, D.J. Joe, K.J. Lee, Part. Part. Syst. Char. 34 (2017) 1600429.
[29] H.M. Jin, D.Y. Park, S.-J. Jeong, G.Y. Lee, J.Y. Kim, J.H. Mun, S.K. Cha, J. Lim, J.S. Kim, K.H. Kim, K.J. Lee, S.O. Kim, Adv. Mater. 29 (2017) 1700595.
[30] J.H. Park, G.-T. Hwang, S. Kim, J. Seo, H.-J. Park, K. Yu, T.-S. Kim, K.J. Lee, Adv. Mater. 29 (2017) 1603473.
[31] F. Lang, O. Shargaieva, V.V. Brus, H.C. Neitzert, J. Rappich, N.H. Nickel, Adv. Mater. 30 (2018) 1702905.
[32] G.A. Elbaz, W.L. Ong, E.A. Doud, P. Kim, D.W. Paley, X. Roy, J.A. Malen, Nano Lett. 17 (2017) 5734.
[33] M.R. Leyden, L. Meng, Y. Jiang, L.K. Ono, L. Qiu, E.J. Juarez-Perez, C. Qin, C. Adachi, Y. Qi, J. Phys. Chem. Lett. 8 (2017) 3193.

[34] N. Onoda-Yamamuro, T. Matsuo, H. Suga, J. Phys. Chem. Solids 51 (1990) 1383.
[35] A. Kovalsky, L. Wang, G.T. Marek, C. Burda, J.S. Dyck, J. Phys. Chem. C 121 (2017) 3228.
[36] B. Wenger, P.K. Nayak, X. Wen, S.V. Kesava, N.K. Noel, H.J. Snaith, Nat. Commun. 8 (2017) 590.
[37] Z. Wang, J.E. Alaniz, W. Jang, J.E. Garay, C. Dames, Nano Lett. 11 (2011) 2206.
[38] H. Dong, B. Wen, R. Melnik, Sci. Rep. 4 (2014) 7037.
[39] J. Favre, D. Fabrègue, E. Maire, A. Chiba, Philos. Mag. A 94 (2014) 1992.
[40] S.J. Kim, J. Byun, T. Jeon, H.M. Jin, H.R. Hong, S.O. Kim, ACS Appl. Mater. Interfaces 10 (2018) 2490.
[41] M.-H. Park, S.-H. Jeong, H.-K. Seo, C. Wolf, Y.-H. Kim, H. Kim, J. Byun, J.S. Kim, H. Cho, T.-W. Lee, Nano Energy 42 (2017) 157.
[42] B. Brunetti, C. Cavallo, A. Ciccioli, G. Gigli, A. Latini, Sci. Rep. 6 (2016) 31896.
[43] L. Hashemi-Sadraei, S.E. Mousavi, E.J. Lavernia, J.M. Schoenung, Adv. Eng. Mater. 17 (2015) 1598.
[44] Z. Wang, T. Cheng, F. Wang, S. Dai, Z. a. Tan, Small 12 (2016) 4412.
[45] S.A. Veldhuis, P.P. Boix, N. Yantara, M. Li, T.C. Sum, N. Mathews, S.G. Mhaisalkar, Adv. Mater. 28 (2016) 6804.
[46] E.J. Juarez-Perez, L.K. Ono, M. Maeda, Y. Jiang, Z. Hawash, Y. Qi, Mater. Chem. 6 (2018) 9604.
[47] K.-H. Wang, L.-C. Li, M. Shellaiah, K. Wen Sun, Sci. Rep. 7 (2017) 13643.
[48] J. Xing, F. Yan, Y. Zhao, S. Chen, H. Yu, Q. Zhang, R. Zeng, H.V. Demir, X. Sun, A. Huan, Q. Xiong, ACS Nano 10 (2016) 6623.
[49] D. Yin, J. Feng, R. Ma, Y.F. Liu, Y.L. Zhang, X.L. Zhang, Y.G. Bi, Q.D. Chen, H.B. Sun, Nat. Commun. 7 (2016) 11573.
[50] J.W. Lee, Y.J. Choi, J.M. Yang, S. Ham, S.K. Jeon, J.Y. Lee, Y.H. Song, E.K. Ji, D.H. Yoon, S. Seo, H. Shin, G.S. Han, H.S. Jung, D. Kim, N.G. Park, ACS Nano 11 (2017) 3311.

Dong Hun Jung received his M.S. (2019) in Materials Science and Engineering from Korea Advanced Institute of Science and Technology (KAIST), Korea. His research focused on the morphology control of perovskite by using light-material interaction. The title of dissertation is “Flash Light Induced Recrystallization of Perovskite for High Efficiency Light-emitting Diodes”. Now he is currently working as an engineer in Samsung Electronics.

Jung Hwan Park received his Ph.D. degree in Materials Science and Engineering from Korea Advanced Institute of Science and Technology (KAIST). During his Ph.D., he pioneered light-material interaction for flexible and stretchable electronics. Currently, he is a postdoctoral research fellow at University of California, Berkeley, in Mechanical Engineering department. His research topic is the novel light-induced materials and devices for wearable electronic system.

Han Eol Lee received his B.S., M.S., and Ph.D. degrees in Materials Science and Engineering (MSE) from Korea Advanced Institute of Science and Technology (KAIST) in 2013, 2015, and 2018, respectively. Currently, he is a BK21 Plus postdoctoral research associate in the Department of Materials Sciences and Engineering at KAIST. His research topics are thin-film microLEDs, flexible/wearable electronics, and laser material interaction for flexible full-color microLED displays.

Jinwoo Byun received his B.S. in Materials Science and Engineering from Yonsei University in 2013 and M.S. degree from Pohang University of Science and Technology (POSTECH) in 2016. Now he is a Ph.D. candidate at Materials Science and Engineering, Korea Advanced Institute of Science and Technology (KAIST). His research interests mainly focus on low dimensional perovskite materials.

Tae Hong Im received his B.S. in Material Science and Engineering (MSE) from Ulsan National Institute of Science and Technology (UNIST) in 2015 and M.S. degree from Korea Advanced Institute of Science and Technology (KAIST) in 2017, respectively. He is currently working toward his Ph.D. and his research topics are light-material interaction for nanomaterial synthesis and flexible display application.

Gil Yong Lee received his B.S. in Advanced Materials Science & Engineering from Sungkyunkwan University in 2012 and M.S. degree from Materials Science and Engineering, Korea Advanced Institute of Science and Technology (KAIST) in 2014. Now he is a Ph.D. candidate at Materials Science and Engineering, Korea Advanced Institute of Science and Technology (KAIST), Korea. His research interests mainly focus on nitrogen-doped carbon nanotube hybrid assembly.

Jae Young Seok received his Ph.D. in Department of Mechanical Engineering from Korea Advanced Institute of Science and Technology (KAIST) in 2019. He is currently a senior researcher at Korea Institute of Machinery and Materials (KIMM) and his research interests include nanostructured electrodes based on metal, carbon, and interfacial oxides for thin film electronics and energy storage devices.

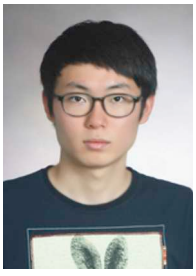

Taeyeong Yun received his Ph.D (2019) in Materials Science and Engineering, Korea Advanced Institute of Science and Technology (KAIST), Korea. Now he is a Post Doc. at Materials Science and Engineering, Korea Advanced Institute of Science and Technology (KAIST), Korea. His research interests mainly focus on two dimensional nanomaterials.

Keon Jae Lee received his Ph.D. in materials science and engineering at University of Illinois, Urbana Champaign (UIUC). During his Ph.D., he was involved in the first co-invention of “flexible single-crystalline inorganic electronics,” using top-down semiconductors and soft lithographic transfer. Since 2009, he has been a pro-fessor in the Department of MSE at KAIST. His current research topics are self-powered flexible electronic systems including energy harvester, IoT sensor, microLEDs, large scale integration, memory, and laser material interaction for biomedical and flexible applications. In addition, he is a cofounder of a spin-off company, FRONICS Ltd., to commercialize his achievements.

Sang Ouk Kim is the Professor in the Department of Materials Science and Engineering at KAIST, and the director of National Creative Research Initiative Center for Multi-Dimensional Directed Nanoscale Assembly and Graphene Liquid Crystalline Fiber Center, Daejeon, Korea. He obtained his Ph.D at KAIST in 2000 and experienced postdoctoral research at University of Wisconsin-Madison, USA. Prof. Kim has published more than 200 SCI journal papers and delivered more than 300 invited presentations thus far. He is the recipient of numerous prestigious awards and serving as an associate editor of Energy Storage Materials and editorial board members for many journals. Prof. Kim's group is actively researching on the nanoscale assembly & chemical modification of various nanomaterials.